10.1098/rspa.2000.0726

THE ROYAL SOCIETY

Polarization patterns of the summer sky and its neutral points measured by full-sky imaging polarimetry in Finnish Lapland north of the Arctic Circle

By József Gál[1], Gábor Horváth[1], Viktor Benno Meyer-Rochow[2] and Rüdiger Wehner[3]

[1]*Department of Biological Physics, Eötvös University, H-1117 Budapest, Pázmány sétány 1, Hungary* (gh@arago.elte.hu)
[2]*Department of Biology (Zoology), University of Oulu, Linnanmaa A, SF-90401 Oulu, Finland* (vmt@sun3.oulu.fi)
[3]*Zoologisches Institut, Universität Zürich, Winterthurerstrasse 190, CH-8057 Zürich, Switzerland* (rwehner@zool.unizh.ch)

Received 6 April 2000; revised 6 November 2000; accepted 30 November 2000

Using 180° field-of-view (full-sky) imaging polarimetry, the patterns of the degree and angle of polarization of the entire summer sky were measured on 25 June 1999 at a location north of the Arctic Circle in Finnish Lapland as a function of the angular solar zenith distance. A detailed description of the used full-sky imaging polarimeter and its calibration is given. A series of the degree and angle of polarization pattern of the full sky is presented in the form of high-resolution circular maps measured in the blue (450 nm) spectral range as a function of the solar zenith distance. Graphs of the spectral dependence of the degree and angle of polarization of skylight at 90° from the Sun along the antisolar meridian are shown. The celestial regions of negative polarization and the consequence of the existence of this anomalous polarization, the neutral points, are visualized. The measured values of the angular zenith distance of the Arago and Babinet neutral points are presented as a function of the zenith distance of the Sun for the red (650 nm), green (550 nm) and blue (450 nm) ranges of the spectrum. The major aim of this work is to give a clear and comprehensive picture, with the help of full-sky imaging polarimetry, of what is going on in the entire polarized skydome. We demonstrate how variable the degree of polarization of skylight and the position of the neutral points can be within 24 h on a sunny, almost cloudless, visually clear day.

Keywords: sky polarization; neutral points; full-sky imaging polarimetry; polarization vision; dispersion of skylight polarization; optical orientation

1. Introduction

The clear sky has a characteristic polarization pattern depending on the angular solar zenith distance (Können 1985). The polarization of skylight has been the subject of numerous theoretical and experimental investigations (e.g. Chandrasekhar

1950; Neuberger 1950; Van de Hulst 1952; Sekera 1957; Holzworth & Rao 1965; Bellver 1987; Coulson 1988; North & Duggin 1997; Voss & Liu 1997; Horváth *et al.* 1998; Horváth & Wehner 1999). Most ground-based measurements of skylight polarization were performed by means of point-source polarimeters using narrow-band interference filters to determine the degree and angle of polarization for different wavelengths of light. As these polarimeters possess a very small aperture (*ca.* 1–5°, in which the optical information is averaged), the polarization characteristics of the sky can be analysed by them only within very restricted fields of view.

The spatial distribution of the degree and angle of polarization of skylight can be determined by scanning the firmament with such a point-source polarimeter, but this is a time-consuming task done rarely and only in special cases. Using a point-source polarimeter and making repeated scans in the Sun's vertical and along a meridian crossing the zenith perpendicularly to the solar meridian, Shaw (1975) measured the polarization of skylight in the blue (400 nm) spectral range during the total solar eclipse of 30 June 1973 in Kenya. Brines & Gould (1982) undertook similar measurements at several points of the firmament by means of a point-source scanning polarimeter. They could measure points at every 5° of zenith distance and azimuth of a half hemisphere of the sky within 7–8 min, during which the Sun moved *ca.* 2° along its arc. Certain unavoidable errors were a consequence of their rapid measurement process, such as inaccuracies attendant upon setting the axes of the instrument. If one wished to enhance the spatial resolution of the samples by one or two orders, to obtain a picture-like scan of the polarization of the entire sky, the measurements would require 70–80 or 700–800 min, a period during which the celestial polarization pattern would change considerably due to the rotation of the Earth (it takes 80 min for the Sun to move by 20°). It is clear that the polarization pattern of the entire firmament cannot reliably be measured by such a time-consuming method. The disadvantage of the very narrow field of view of point-source polarimeters can be eliminated by wide-field-of-view imaging polarimetry.

The fields of view of the different imaging polarimeters designed for different purposes by Walraven (1981), Prosch *et al.* (1983), Egan (1986), Wolff (1994), Deschamps *et al.* (1994), Cronin *et al.* (1994), Shashar *et al.* (1995), Horváth & Zeil (1996), Horváth & Varjú (1997), Horváth *et al.* (1997, 1998) or Horváth & Wehner (1999), for example, are limited by the field of view of the (video or photo) camera used, being generally no larger than *ca.* 40–50°. The entire celestial hemisphere cannot be recorded with these polarimeters. Recently, North & Duggin (1997) developed a practical method for obtaining partial Stokes vectors and derivative images of the firmament by taking advantage of a four-lens photographic camera. Although the spherical convex mirror of their imaging polarimeter possessed a field of view of almost 180°, they could not record the entire skydome, because the camera of their equipment was set up on a huge, heavy tetrapod at a height of 6 m above the mirror. The tetrapod, and also the camera itself, screened out small areas of the firmament. Furthermore, this equipment was rather voluminous and cumbersome, which did not permit easy and rapid setting up, taking down, transfer and transport. Another, much easier but unportable, design was developed by Voss & Liu (1997) for measuring the distribution of polarization in the full sky. The charge-coupled device image sensor (detector) of this full-sky imaging polarimeter should be thermoelectrically cooled ($-40 \leqslant T \leqslant -30\,^{\circ}\mathrm{C}$), and the instrument needs a power supply (220 or 110 V) and connection with a computer.

Using 180° field-of-view imaging polarimetry, an opportunity to measure the polarization pattern of the entire summer sky occurred for us in Finnish Lapland north of the Arctic Circle. The major motivation of our study was to give a clear and comprehensive picture of what is going on in the entire polarized skydome. Since full-sky scans of the polarization of skylight have not previously been undertaken, this work fills this gap. In the present work we first describe in detail our instrument and its calibration. Then we show a series of the degree and angle of polarization patterns of the full sky in the form of high-resolution circular maps measured in the blue (450 nm) spectral range as a function of the angular solar zenith distance. Graphs of the spectral dependence of the degree and angle of polarization of skylight at 90° from the Sun along the antisolar meridian are presented. The celestial regions of negative polarization and the consequence of the existence of this anomalous polarization, the neutral points, are visualized. The measured values of the angular zenith distance of the Arago and Babinet neutral points are given as a function of the solar zenith distance for the red (650 nm), green (550 nm) and blue (450 nm) ranges of the spectrum. Since at the place and time of our measurements the Sun did not set, we could measure the 24 h change of the polarization pattern of the summer sky. We demonstrate here how variable the degree of polarization of skylight and the position of the neutral points can be within 24 h on a sunny, almost cloudless, visually clear day.

2. Materials and methods

(*a*) *Place and date of the measurements*

Our measurements were carried out on a sunny day (25 June 1999) at Sodankylä Meteorological Station (67°25′ N, 26°30′ E) of the University of Oulu (Finland) from 02:00 on 25 June 1999 to 01:00 on 26 June 1999 (the latter point of time is called the '25th hour' further on in this work). The station is located in the vicinity of the township of Sodankylä in Finnish Lapland, north of the Arctic Circle. We measured the polarization pattern of the entire celestial hemisphere from the top of a 16 m high meteorological tower rising above the tips of the surrounding pine trees.

The tower was in the middle of a huge pine forest, the trees of which did not disturb our recordings. The spatial distribution of the albedo of the surrounding terrain (pine forest) was homogeneous, and there was no spatio-temporal variation of the local albedo during our measurements. Since at the place and time of our measurements the Sun did not set, we could make hourly measurements of the changing polarization pattern of the summer sky throughout the whole day (from 0 to 24 h, local summer time = UTC + 3). During our measuring campaign, the sky was relatively clear for almost the entire day, but sometimes high altitude thin cirrus clouds occurred near the horizon.

(*b*) *Measurement of the celestial polarization pattern by full-sky imaging polarimetry*

The set-up of our full-sky rotating-analyser imaging photopolarimeter is shown in figure 1*a*. An angle of view of 180° is ensured by a Nikon–Nikkor fish-eye lens (F-number = 2.8, focal length = 8 mm), including a built-in rotating disc mounted with three neutral density linearly polarizing (HNP'B) filters with three different

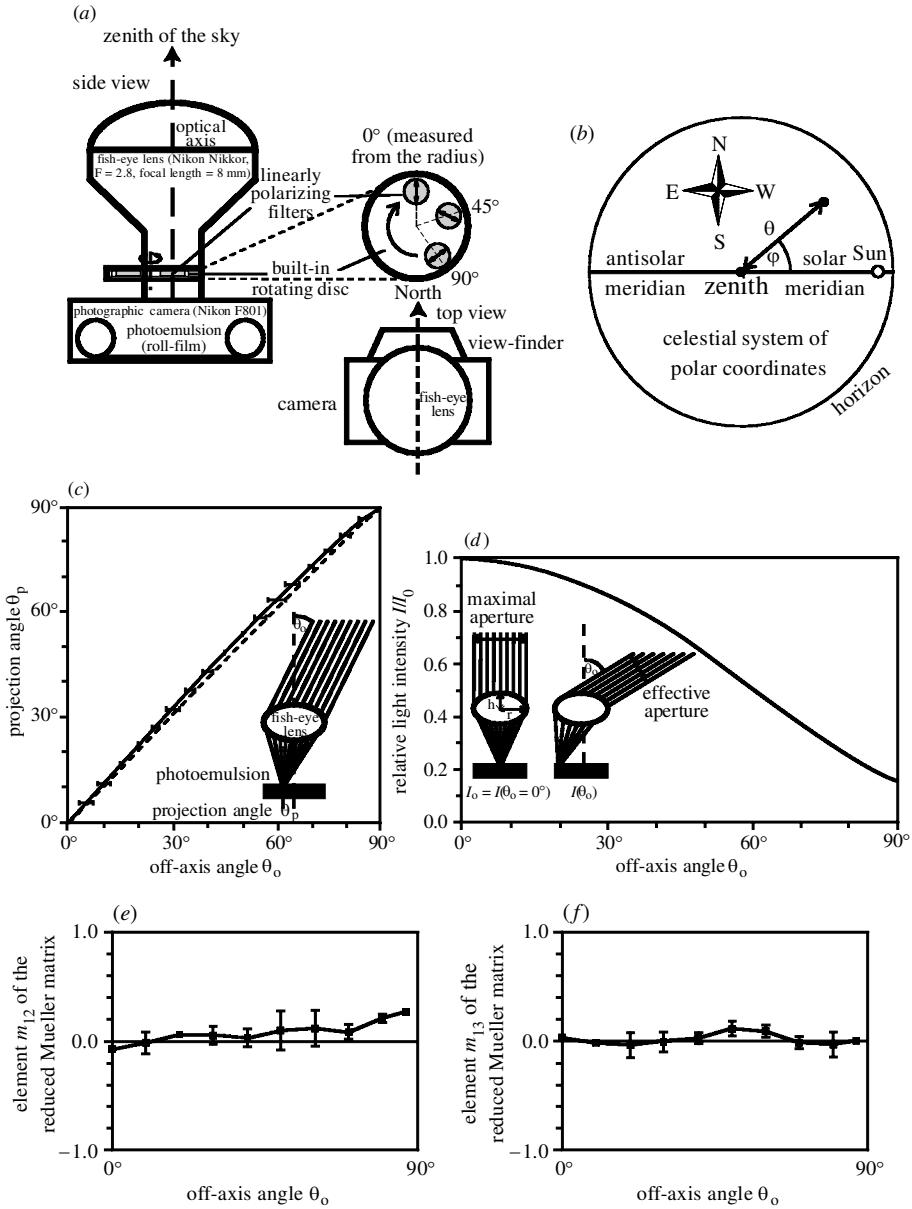

Figure 1. (*a*) Schematic representation of the 180° field-of-view (full-sky) rotating-analyser imaging photopolarimeter in side and top view. The direction of the transmission axis of the polarizing filters is indicated by double-headed arrows. (*b*) The celestial polar-coordinate system used in the representation of the sky polarization patterns. (*c*)–(*f*) Optical characteristics of the imaging polarimeter. (*c*) Relationship between the off-axis angle θ_o and the projection angle θ_p projected onto the photoemulsion by the fish-eye lens. The dashed straight line represents the ideal case when $\theta_o = \theta_p$. (*d*) Decrease of the light intensity $I(\theta_o)$ on the photoemulsion because of the decrease of the effective aperture versus θ_o. The maximum of I is $I_0 = I(\theta_o = 0)$, with maximal aperture of the fish-eye lens. (*e*), (*f*) Change of the elements m_{12} and m_{13} of the reduced Mueller matrix of the fish-eye lens as a function of θ_o.

polarization axes (0, 45 and 90°, measured from the radius of the disc), and the detector is a photoemulsion in a Nikon F801 photographic camera. For the detector, we used Fujichrome Sensia II 100 ASA colour reversal film; the maxima and half band widths of its spectral sensitivity curves were $\lambda_{\mathrm{red}} = 650 \pm 30$, $\lambda_{\mathrm{green}} = 550 \pm 30$ and $\lambda_{\mathrm{blue}} = 450 \pm 50$ nm.

From a given sky, three photographs were taken for the three different alignments of the transmission axis of the polarizers on the built-in rotating disc. The camera was set up on a tripod in such a way that its axis passing through the viewfinder pointed northward and the optical axis of the fish-eye lens was vertical, pointing towards the zenith (figure 1*a*). In order to eliminate distorting internal reflections of direct sunlight from the refracting surfaces of the fish-eye lens, the Sun was screened out by a small disc, which could be slid along a circular wire positioned radially and concentrically with respect to the outer (entrance) surface of the lens.

The reliability of the process of development of the colour reversal films was ensured by always developing the films in the same professional Kodak photographic laboratory (in Budapest), using the same automatically controlled method. With the aid of a personal computer, after an eight-bit (true-colour) digitization (with a Hewlett Packard ScanJet 6100C with an optical resolution of 600 dpi and an enlargement (or scaling) of 500%) and evaluation of the three developed colour slides belonging to a given sky, the patterns of the brightness, degree and angle of polarization of skylight were determined and visualized as high-resolution colour-coded two-dimensional circular maps in the red (650), green (550) and blue (450 nm) spectral ranges, in which the three colour-sensitive layers of the used photoemulsion have the maximal sensitivity. The red, green and blue spectral ranges were obtained using a digital image processing program provided with the scanner to digitally separate the colour channels in the digitized images. The calculation of the brightness, degree and angle of polarization of skylight was the same as in the case of videopolarimetry (Horváth & Varjú 1997). The three-dimensional celestial hemisphere was represented in two dimensions by a polar-coordinate system, where the angular distance θ from the zenith and the azimuth angle φ from the solar meridian are measured radially and tangentially, respectively (figure 1*b*). In this two-dimensional coordinate system, the zenith corresponds to the centre and the horizon to the perimeter of the circular map.

(*c*) *Algorithmic determination of the zenith distance of the Arago and Babinet neutral points*

In the red, green and blue spectral ranges, the zenith distances of the Arago and Babinet neutral points were determined by a simple algorithm, which took into consideration that (i) the skylight is unpolarized ($\delta = 0\%$) in a neutral point; (ii) the degree of polarization gradually increases with increasing angular distance from a neutral point; and (iii) the skylight polarization switches from negative to positive (that is, the angle of polarization α suffers a change of $|\Delta\alpha| = 90°$) as one passes a neutral point parallel to the solar or antisolar meridian. The points possessing these characteristics were recognized in a given sky (around the tips of the eight-shaped blue-green celestial region of the α-pattern with positive polarization seen in figure 2*a*). Then the position of the Arago or Babinet point was obtained as the geometric centre (centre of mass) of these points. In certain cases, the deviation of

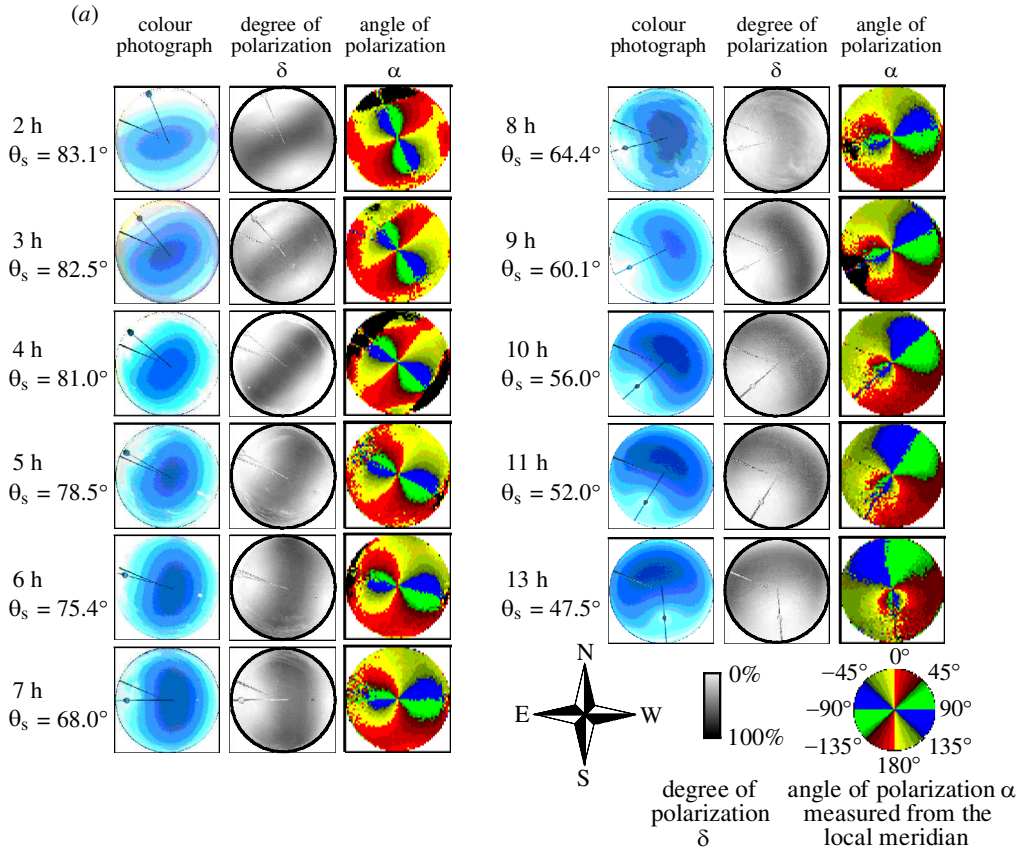

Figure 2. (*a*) The colour photograph and the degree δ and angle α of polarization pattern of the entire celestial hemisphere versus the time (and the angular solar zenith distance θ_s) measured by full-sky imaging polarimetry in the blue (450 nm) spectral region from 2 h (local summer time = UTC + 3, $\theta_s = 83.1°$) to 13 h ($\theta_s = 47.5°$) on 25 June 1999 in Sodankylä (67°25′ N, 26°30′ E, Finnish Lapland). In the black celestial regions of the α-pattern, the photoemulsion was over-exposed. The two radial bars in the circular pictures come from a wire (holding a small disc to screen out the Sun) and a pole (pointing approximately north-eastward and accommodating an anemometer) on the top of the meteorological tower where the measurement was performed. The position of the Sun is indicated by the small screening disc.

these points from each other was so great that the Arago and/or the Babinet neutral point could not have been algorithmically recognized. This is the reason why the positions of the Arago and Babinet points could not always have been evaluated from the measured celestial polarization patterns (figure 3).

(*d*) *Instrument calibration*

The calibration of our instrument involved the determination of the influence of the fish-eye objective on the optical parameters of the light passing through it, and the determination of the transfer function of the whole evaluation process; that is, the function between the real intensity I of the light fallen onto the photoemulsion and the digital value DV of the brightness taken from the digitization process.

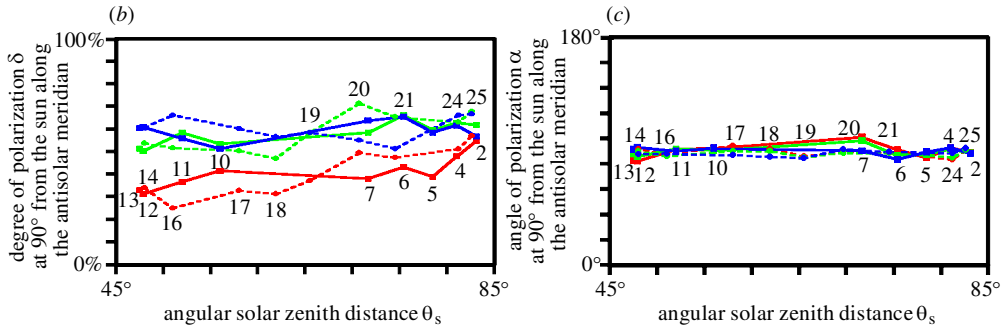

Figure 2. (*Cont.*) (*b*), (*c*) Spectral dependence of the degree δ and angle α of polarization of skylight measured in the blue (450), green (550) and red (650 nm) spectral ranges at 90° from the Sun (averaged on a small circular celestial region with a radius of ten pixels; the radius of the entire sky was 334 pixels) along the antisolar meridian versus the angular solar zenith distance θ_s. The numbers around the graphs indicate the hours (UTC + 3) of recording. In the first and second half of the course, the neighbouring points of the graphs are connected with solid and broken straight lines (linear interpolation), respectively.

(i) *Calibration of the fish-eye objective*

Our 180° field-of-view fish-eye objective forms a circular image with a radius of $R = 10$ mm in its focal plane (on the photoemulsion) from the object field. The incident rays originating from a given off-axis angle θ_o are focused into a given point of this circular image at a distance r from the centre. The value of the so-called 'projection angle' was calculated as $\theta_p = 90°r/R$. In order to determine the angular transfer function $\theta_o(\theta_p)$ of the camera-fish-eye lens system, we took pictures from an arc composed of a black and white grating with a frequency of 5° in its centre with the fish-eye lens and the camera. The measured inverse angular transfer function $\theta_p(\theta_o)$ is shown in figure 1*c*. The polynomial fitted to the measured values of $\theta_o(\theta_p)$ is

$$\left.\begin{aligned} \theta_o &= \left[\sum_{i=1}^{7} a_i \cdot \left(\frac{\theta_p}{90°}\right)^i\right] 90°, \\ a_1 = 0.977\,552, &\quad a_2 = -0.862\,213, \quad a_3 = 5.405\,678, \\ a_4 = -16.3937, &\quad a_5 = 26.219\,318, \quad a_6 = -20.857\,125, \\ a_7 = 6.510\,49, &\quad 0 \leqslant \theta_p \leqslant 90°, \quad \theta_o = \theta_o(\theta_p). \end{aligned}\right\} \tag{2.1}$$

The light intensity I reaching the photoemulsion decreases because of the decrease in the effective aperture as the off-axis angle θ_o increases. The change of the relative light intensity I/I_0 versus θ_o is as follows (figure 1*d*):

$$\left.\begin{aligned} \frac{I(\theta_o)}{I(\theta_o = 0)} \equiv \frac{I}{I_0} &= \cos\theta_o \qquad \text{if } \theta_o \leqslant \arctan\left(\frac{\rho - h}{r}\right), \\ \frac{I}{I_0} &= \frac{1}{2r}\left[r\cos\theta_o + \frac{r^2 + h^2}{2h}(1 - \sin\theta_o) + h\sin\theta_o\right] \\ &\qquad \text{if } \theta_o > \arctan\left(\frac{\rho - h}{r}\right), \end{aligned}\right\} \tag{2.2}$$

where $I_0 = I(\theta_o = 0)$ is the maximum of $I(\theta_o)$, when the incident rays of light are parallel to the optical axis, and $r = 53$, $h = 16$ and $\rho = 96$ mm are the radius of the aperture and the height and the radius of curvature of the entrance surface of the fish-eye lens, respectively (see the inset in figure 1*d*).

In order to determine the change of the optical properties of the light passing through the fish-eye objective (without polarizing filter), we have to know its system Mueller matrix $\boldsymbol{M}(\theta_o)$ as a function of the off-axis angle θ_o. In general, this means that we have to know the functions of all of its 16 elements: $M_{11}(\theta_o), M_{12}(\theta_o), \ldots, M_{44}(\theta_o)$. However, in the case of our full-sky imaging polarimeter, we do not need all of these elements. The reasoning behind this is as follows (cf. Voss & Liu 1997):

(i) Since the photoemulsion is sensitive only to the intensity of the incoming light, only the first row (M_{11}, M_{12}, M_{13}, M_{14}) of the total system Mueller matrix must be determined.

(ii) In general, the light in the atmosphere is not circularly polarized (Coulson 1988), so we do not need to measure this quantity.

(iii) According to the standard calibration methods of polarimetry (Azzam & Bashara 1989), we used the so-called reduced Mueller matrix $\boldsymbol{m}$, which is the system Mueller matrix normalized to M_{11} ($m_{ij} = M_{ij}/M_{11}$).

Consequently, it was enough to determine only the spectral and spatial characteristics and the elements $m_{12}(\theta_o)$ and $m_{13}(\theta_o)$ of the reduced Mueller matrix. For the radiometric scalar (non-polarized) calibration of our camera-fish-eye lens system, we used the method described by Voss & Zibordi (1989). We measured the elements $m_{12}(\theta_o)$ and $m_{13}(\theta_o)$ of the reduced Mueller matrix (figure 1*e*, *f*) with standard methods (Azzam & Bashara 1989).

(ii) *Calibration of the evaluation process*

In the calibration of the evaluation process of our full-sky imaging polarimetry we have considered the following characteristics.

(i) The spectral properties and Mueller matrix of the built-in HNP'B linearly polarizing filters, available from the standard catalogue of the manufacturer, Polaroid Europe Ltd (Uxbridge, Middlesex, UK).

(ii) The spectral sensitivity and density ($D = \log(I_{\text{incoming}}/I_{\text{passing}})$ in the red (650), green (550) and blue (450 nm) spectral ranges) curves of the photoemulsion given in the standard catalogue of the manufacturer, Fuji Photo Film Company Ltd (Tokyo, Japan).

(iii) To determine the transfer function between the density D and the digital value DV of the brightness obtained after the digitization process, we used several test slides of different densities.

The density of a given test slide was measured by a scanning spectrometer (Shimadzu UV-2101PC) in the spectral range 400–800 nm. After scanning these test slides, we could determine the $DV(D)$ function. Using the spectral sensitivity curves, the density functions $D(I)$ (available from the manufacturer's catalogue) and the $DV(D)$

functions (in the red, green and blue channels), we could determine the $DV(I)$ functions (depending on the type of the photoemulsion used as detector). From the inverse $I(DV)$ function, we could calculate the real intensity of light I (measured in lux seconds (lx s)).

3. Results

Figure 2*a* shows a series of the colour photographs and the degree δ and angle α of polarization patterns of the entire celestial hemisphere as a function of the angular solar zenith distance θ_s measured by full-sky imaging polarimetry in the blue (450 nm) spectral range from $\theta_s = 83.1$ to $\theta_s = 47.5°$ on 25 June 1999 in Sodankylä (67°25′ N, 26°30′ E, Finnish Lapland). Because of the qualitative resemblance of the full-sky polarization patterns measured in different spectral ranges, we omit the patterns measured in the red and green ranges.

In figure 2*a* we can see, for example, that the degree of skylight polarization first increases with increasing angular distance from the Sun, reaching its maximum, the value of which depends on the Sun's zenith distance and on the meteorological conditions (on haze and the aerosol concentration), at *ca.* 90° from the Sun, and then decreasing towards the anti-Sun. The δ-pattern at 8 h demonstrates how the degree of polarization of skylight was reduced by the thin cirrus clouds near the horizon. Figure 2*a* demonstrates well the characteristic axial symmetry of the sky polarization pattern too, and that the axis of symmetry is the solar and antisolar meridian.

Parts (*b*) and (*c*) of figure 2 show the spectral dependence of the degree δ and angle α of polarization of skylight measured in the blue (450), green (550) and red (650 nm) spectral ranges at 90° from the Sun along the antisolar meridian as a function of the angular solar zenith distance. Sky polarization is frequently measured in this celestial direction, where δ is maximal θ if the sky is clear. We can see from figure 2*b* that, during the 24 h period investigated (from 2 to 24 + 1 h), at 90° from the Sun along the antisolar meridian, the degree of polarization of skylight was always lowest in the red spectral range ($25 \leqslant \delta_{red} \leqslant 57\%$ for solar zenith distances of $47.5 \leqslant \theta_s \leqslant 83.1°$). For certain solar zenith distances, the δ values were higher in the blue spectral range than those in the green range, while for other solar zenith distances the relation was the contrary. Although the temporal change of the degree of polarization δ was not monotonous in all three spectral ranges, there was a general trend that, at 90° from the Sun, δ decreased with decreasing solar zenith distance, especially in the red region of the spectrum. During the 24 h studied, there was a characteristic hysteresis in the temporal change of the degree of polarization: when the Sun moved along the first half of its arc, from 2 to 13 h, the change of δ in all three spectral ranges was characterized by different graphs in comparison with the case between 14 and 24 + 1(= 25) h.

We can see in figure 2*c* that, during the 24 h period studied, at 90° from the Sun along the antisolar meridian, independently of the wavelength, the angle of polarization was always within the range $80 < \alpha < 100°$, with an average of $90 \pm 10°$; that is, the direction of polarization was always approximately perpendicular to the antisolar meridian, as expected from Rayleigh theory. The difference between the α values at a given time was maximal for the red and blue range of the spectrum and it was always smaller than *ca.* 10°. There was not any systematic temporal change of the angle of polarization.

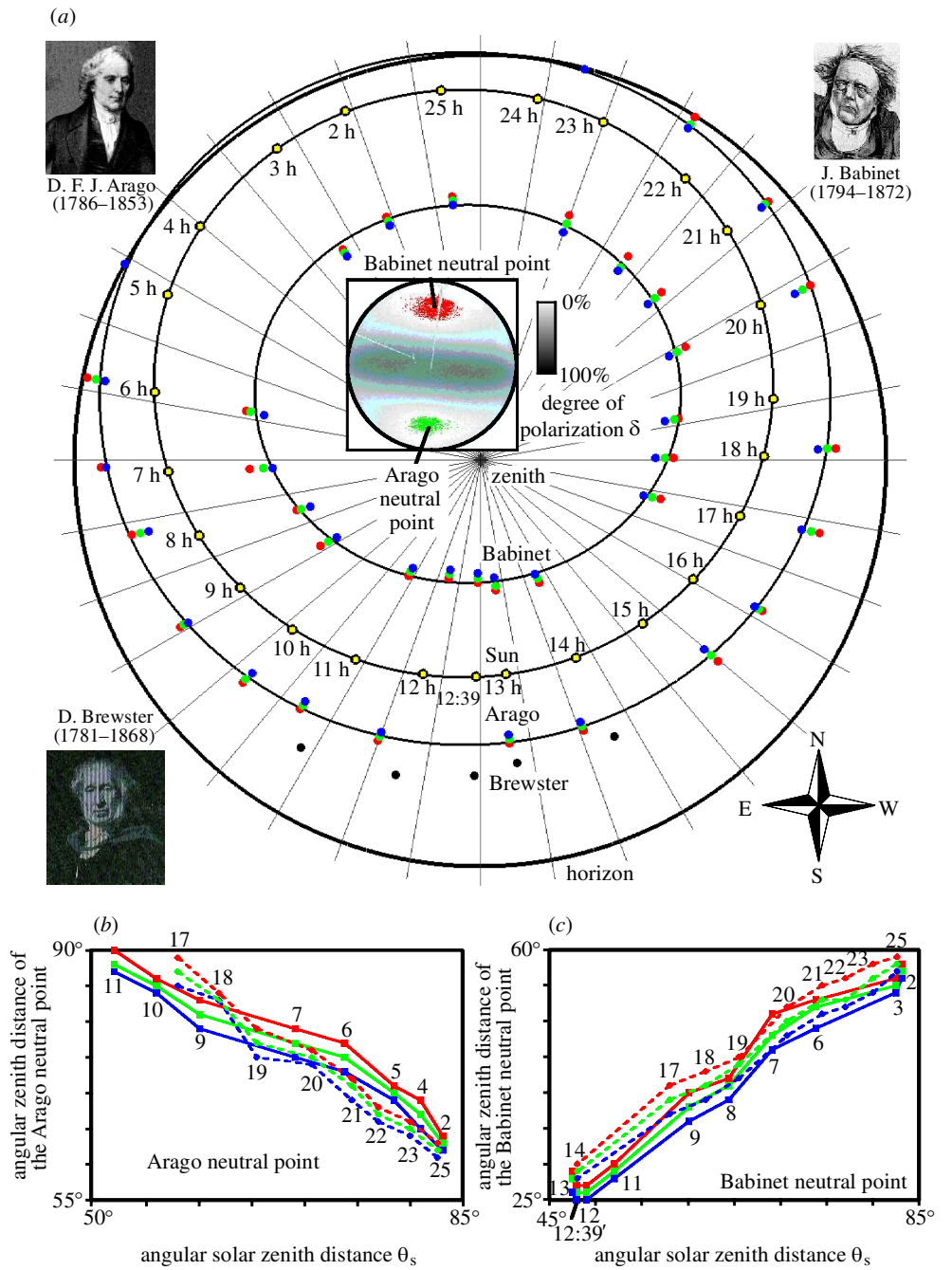

Figure 3. For description see opposite.

In the patterns of the angle of polarization in figure 2*a*, the α values ranging between -45 and $+45°$ (that is, more or less parallel to the local meridian) are represented by red and yellow colours, while green and blue colours represent $45 <$

$\alpha < 135°$ (that is, more or less perpendicular to the local meridian). We can see that, in the case of this colour coding of the angle of polarization, an eight-shaped blue–green region occurs around the zenith in the dominating yellow–red area of the sky. The bright yellow–red zones around the tips of this eight-shaped blue–green region are the areas of the so-called 'anomalous' or 'negative' polarization of skylight. The polarization along the solar and antisolar meridian within this blue–green eight-shaped celestial region is called 'normal' or 'positive'. Figure 2*a* demonstrates well how the celestial areas of positive and negative polarization change as a function of the solar zenith distance.

The consequence of the negative polarization of skylight is the existence of the unpolarized or neutral points. The Arago and Babinet neutral points are positioned always at the tips of the eight-shaped blue–green region of the angle of polarization maps in figure 2*a*, where positive polarization switches to negative polarization. Figure 3*a* represents the hourly positions of the Arago and Babinet neutral points of skylight polarization on the firmament evaluated from a 24 h series of the celestial polarization patterns measured by full-sky imaging polarimetry on 25 June 1999 in Sodankylä in the red (650), green (550) and blue (450 nm) spectral ranges. The positions of the Brewster neutral point could not have been evaluated due to the over-exposure of the photoemulsion in the vicinity of the Sun. Usually, the Brewster point is positioned on the solar meridian below the Sun at about the same angular distance as the Babinet point above the Sun (Coulson 1988; Horváth *et al.* 1998). The positions of the Brewster neutral point (indicated by black dots in figure 3*a*) were predicted on the basis of this rule.

The inset in the middle of figure 3*a* shows the pattern of the degrees of polarization δ for a solar zenith distance of $\theta_s = 81.2°$ measured at 24 h (UTC+3) on 25 June 1999 in Sodankylä. The Arago and Babinet neutral points and their immediate vicinities are shaded with green and red colours, respectively, indicating $\delta \leqslant 2\%$. Parts (*b*) and (*c*) of figure 3 represent the change of the zenith distance of the Arago and Babinet neutral points for the red, green and blue spectral ranges as a function of the solar zenith distance. The most important characteristics of the Arago and Babinet points read from figure 3 are the following.

Figure 3. (*a*) Hourly positions of the Sun and Arago, Babinet and Brewster neutral points of skylight polarization on the firmament evaluated from a 24 h series of the celestial polarization patterns measured by full-sky imaging polarimetry on 25 June 1999 in Sodankylä. The positions of the Sun are indicated by yellow dots, and next to them the times of recording are shown. The positions of the Arago and Babinet neutral points measured in the red (650), green (550) and blue (450 nm) spectral regions are indicated by red, green and blue dots, respectively. At a given position of the Sun, the Babinet point is placed on the solar meridian, while the Arago point is placed on the antisolar meridian. Black dots represent the predicted positions of the Brewster neutral point. For a few hours, the positions of the Arago and Babinet points could not be evaluated from the recordings. The ellipses represent the trajectories of the Sun and the Arago and Babinet points fitted to their hourly measured positions by the method of least squares. The insets in the corners show the portraits of Arago, Babinet and Brewster, who discovered the neutral points of the polarized firmament in 1810, 1840 and 1842, respectively. The inset in the middle shows the pattern of the degree of polarization δ of the full sky for an angular solar zenith distance of $\theta_s = 81.2°$, measured at 24 h on 25 June 1999 in Sodankylä, where the Arago and Babinet neutral points and their immediate vicinities are shaded with green and red colours, respectively, indicating $\delta \leqslant 2\%$. (*b*), (*c*) The change of the angular zenith distance of the Arago and Babinet neutral points for the red, green and blue spectral ranges as a function of the angular solar zenith distance. The numbers around the graphs indicate the hours (local summer time, UTC + 3) of recording. In the first and second half of the course, the neighbouring points of the graphs are connected with solid and broken straight lines (linear interpolation), respectively.

(i) The smaller the solar zenith distance, the smaller or the larger is the zenith distance of the Babinet or Arago point, respectively.

(ii) The longer the wavelength of skylight, the larger is the zenith distance of the Arago and Babinet points.

Similarly to the temporal change of the degree of polarization of skylight at 90° from the Sun, during the 24 h studied, there was a hysteresis in the temporal change of the zenith distance of the Arago and Babinet points, as can be seen in figure 3*b*, *c*. When the Sun moved along the first half of its arc in the sky (from 2 to 11 h for the Arago point, and from 2 to 13 h for the Babinet point), the change of the zenith distance of the neutral points in all three spectral ranges was characterized by different graphs, in comparison with the case when the Sun moved along the second half of its arc (from 17 to 25 h for the Arago point, and from 14 to 25 h for the Babinet point).

4. Discussion

In our full-sky imaging polarimetric method, we used a normal photographic camera with roll-films. For this purpose, one can also use a digital camera with an appropriate fish-eye lens with a 180° field of view. The use of a photoemulsion in a normal camera and a digitizing system (e.g. a scanner) with a high optical resolution has the advantage that, at least presently, a much greater spatial resolution can be achieved than in the case of a digital camera. Furthermore, for field work, conventional photographic cameras are more advantageous than digital cameras, which are very sensitive to environmental variations, such as dust, direct sunshine, or changes in air temperature, air humidity or electromagnetic fields, for example. Digital cameras also need expensive electromagnetic storage media, or a connection to a portable computer, in order to store the digital recordings. The latter method of information storage is not ideal for field work. These problems are simply eliminated if one uses a normal and less sensitive photographic camera with as many roll-films as needed in the field.

Figures 2*b* and 3 demonstrate that the degree of polarization of skylight and the zenith distance of the neutral points of skylight polarization can change considerably within hours even if the sky is relatively visually clear throughout the day (24 h). The rather unsettled temporal variation of the degree of polarization of the clear sky and the hysteresis of this variation seen in figure 2*b* and figure 3*b*, *c*, show that the degree of polarization pattern of a clear sky is temporally unstable (that is, for the same solar zenith distance at different times, significantly different δ values can occur in a given point of a clear sky), in comparison with the relatively stable pattern of the angle of polarization (that is, the α values in a given point of a clear sky are approximately the same at different times if the solar zenith distance is the same). This problem, and the temporal stability of the α-pattern of a cloudy sky, are studied and discussed elsewhere (Pomozi *et al.* 2001). Thus it is not surprising that polarization-sensitive animals that orient or navigate with the aid of the celestial polarization use the angle of polarization pattern of the sky and not the degree of polarization pattern (Wehner 1976, 1997; Brines & Gould 1982).

The most anomalous feature for figure 2*b* is the low magnitude of the degree of polarization in the red (650 nm) spectral range. This corresponds to that measured by Coulson (1988, pp. 308–312) at Davis (CA, USA), under conditions of moderate haze on 25 July 1973, for instance. The surface albedo of the area surrounding Davis

is typical of that of green vegetation, with some fields of bare loam-type soil, like the area surrounding Sodankylä, the place of our imaging polarimetric measurements. A decrease in the degree of polarization of skylight at the longer wavelengths is typical of hazy conditions, and the relatively high albedo of vegetated surfaces (pine forest in Sodankylä) in the longer wavelength range is an additional contributing factor. Generally, the turbidity (e.g. haze or dust) of the atmosphere strongly reduces the maximum of the degree of polarization, particularly at longer wavelengths (Coulson 1988, p. 289). This may also explain why northern Finnish bumblebees exhibit highest polarization sensitivity in the blue-sensitivity photoreceptor cells (Meyer-Rochow 1981).

Using a point-source polarimeter, Beaglehole & Carter (1992) measured the skylight polarization in the Sun-zenith plane in a high-albedo environment in the Antarctic during spring. They experienced that the skylight in Antarctica had a low maximum polarization of *ca.* 40%, essentially independent of wavelength across the visible spectrum due to multiple scattering in the atmosphere induced by the high snow albedo. Contrary to these findings, at Sodankylä we observed a greater spectral variation of the degree of polarization δ of skylight and higher maxima of δ ranging from 25 to 72% (figure 2*b*). The zenith distance of the Arago and Babinet neutral points also depended on the wavelength (figure 3). These observations can be explained by the fact that our measurements were performed in summer in a pine forest and not in a snowy high-albedo environment. Thus the spectral characteristics of the sky polarization in Sodankylä were influenced less by the multiple scattering in the atmosphere induced by light reflected from the woody terrain.

For a neutral point to occur in the sky, the positively polarized skylight intensity (the Stokes parameter Q if $U = 0$), in which the direction of polarization is normal to the plane of scattering passing through the observer, the Sun and the point observed, should be cancelled out by the negatively polarized skylight intensity, in which the direction of polarization is parallel to the scattering plane. Multiple scattering of light enhances the negatively polarized intensity (Chandrasekhar 1950). The stronger the multiple scattering, the greater the negatively polarized intensity that appears in the atmosphere, and the more the neutral points are displaced from the Sun or anti-Sun. The amount of multiple scattering is strongly affected by atmospheric turbidity.

The different positions of the neutral points in the red, green and blue regions of the spectrum seen in figure 3 demonstrate well the dispersion of skylight polarization and are in accordance with earlier measurements (Coulson 1988; Horváth *et al.* 1998). Können (1985), in his popular book about polarized light in nature, and Coulson (1988), in his famous monograph on polarization and intensity of light in the atmosphere, summarized information on skylight polarization put together during the last two centuries. These studies are now complemented by the direct measurements and the visualization of the polarization patterns of the entire celestial hemisphere with the aid of full-sky imaging polarimetry. The advantage of this approach lies in the ability to image the polarization of the entire sky, and to produce high-resolution colour-coded circular maps of the degree and angle of polarization of skylight. Finally, we would like to mention that using an appropriate waterproof housing, 180° field-of-view imaging polarimetry can also be used underwater to measure the extended polarization patterns of aquatic optical environments.

This work was supported by a three-year János Bolyai postdoctoral research fellowship received by G.H. from the Hungarian Academy of Sciences, and by a one-year doctoral research fel-

lowship received by J.G. from the George Soros Foundation (grant number 230/2/878). The grants OTKA T-034981 received by G.H. from the Hungarian National Science Foundation and 31-43317.95 received by R.W. from the Swiss National Science Foundation are gratefully acknowledged. Further financial support came from the Oulu University and Nowotka Metallbau K G, Bremen (V.B.M.-R.). Many thanks are due to Professor Jorma Kangas (Sodankylä Geophysical Observatory), who organized our accommodation at the Meteorological Station in Sodankylä. We are grateful to two anonymous referees for their valuable comments.

References

Azzam, R. M. A. & Bashara, N. M. 1989 *Ellipsometry and polarized light*. Amsterdam: North-Holland.

Beaglehole, D. & Carter, G. G. 1992 Antarctic skies. 2. Characterization of the intensity and polarization of skylight in a high albedo environment. *J. Geophys. Res.* **97**, 2597–2600.

Bellver, C. 1987 Influence of particulate pollution on the positions of neutral points in the sky at Seville (Spain). *Atmos. Environ.* **21**, 699–702.

Brines, M. L. & Gould, J. L. 1982 Skylight polarization patterns and animal orientation. *J. Exp. Biol.* **96**, 69–91.

Chandrasekhar, S. 1950 *Radiative transfer*. Oxford: Clarendon.

Coulson, K. L. 1988 *Polarization and intensity of light in the atmosphere*. Hampton, VA: A. Deepak.

Cronin, T. W., Shashar, N. & Wolff, L. B. 1994 Portable imaging polarimeters. In *Proc. 12th IAPR Int. Conf. on Pattern Recognition, Jerusalem, Israel, 9–13 October 1994*, pp. 606–609.

Deschamps, P. Y., Bréon, F. M., Leroy, M., Podaire, A., Bricaud, A., Buriez, J. C. & Séze, G. 1994 The POLDER mission: instrument characteristics and scientific objectives. *IEEE Trans. Geosci. Remote Sensing* **32**, 598–615.

Egan, W. G. 1986 Proposed design of an imaging spectropolarimeter/photometer for remote sensing of earth resources. *Opt. Engng* **25**, 1155–1159.

Holzworth, G. C. & Rao, C. R. 1965 Studies of skylight polarization. *J. Opt. Soc. Am.* **55**, 403–408.

Horváth, G. & Varjú, D. 1997 Polarization pattern of freshwater habitats recorded by video polarimetry in red, green and blue spectral ranges and its relevance for water detection by aquatic insects. *J. Exp. Biol.* **200**, 1155–1163.

Horváth, G. & Wehner, R. 1999 Skylight polarization as perceived by desert ants and measured by video polarimetry. *J. Comp. Physiol.* A **184**, 1–7.

Horváth, G. & Zeil, J. 1996 Kuwait oil lakes as insect traps. *Nature* **379**, 303–304.

Horváth, G., Gál, J. & Wehner, R. 1997 Why are water-seeking insects not attracted by mirages? The polarization pattern of mirages. *Naturwissenschaften* **84**, 300–303.

Horváth, G., Gál, J., Pomozi, I. & Wehner, R. 1998 Polarization portrait of the Arago point: video-polarimetric imaging of the neutral points of skylight polarization. *Naturwissenschaften* **85**, 333–339.

Können, G. P. 1985 *Polarized light in nature*. Cambridge University Press.

Meyer-Rochow, V. B. 1981 Electrophysiology and histology of eye of the bumblebee *Bombus hortorum* (Hymenoptera: Apiolae). *J. R. Soc. NZ* **11**, 123–153.

Neuberger, H. 1950 Arago's neutral point: a neglected tool in meteorological research. *Bull. Am. Meteorol. Soc.* **31**, 119–125.

North, J. A. & Duggin, M. J. 1997 Stokes vector imaging of the polarized sky-dome. *Appl. Opt.* **36**, 723–730.

Pomozi, I., Horváth, G. & Wehner, R. 2001 How the clear-sky angle of polarization pattern continues underneath clouds: full-sky measurements and implications for animal orientation. *J. Exp. Biol.* (In the press.)

Prosch, T., Hennings, D. & Raschke, E. 1983 Video polarimetry: a new imaging technique in atmospheric science. *Appl. Opt.* **22**, 1360–1363.

Sekera, Z. 1957 Light scattering in the atmosphere and the polarization of skylight. *J. Opt. Soc. Am.* **47**, 484–490.

Shashar, N., Cronin, T. W., Johnson, G. & Wolff, L. B. 1995 Portable imaging polarized light analyzer. *Proc. SPIE* **2426**, 28–35.

Shaw, G. E. 1975 Sky brightness and polarization during the 1973 African eclipse. *Appl. Opt.* **14**, 388–394.

Van de Hulst, H. C. 1952 Scattering in atmospheres. In *The atmosphere of the earth and planets* (ed. G. P. Kniper). University of Chicago Press.

Voss, K. J. & Liu, Y. 1997 Polarized radiance distribution measurements of skylight. I. System description and characterization. *Appl. Opt.* **36**, 6083–6094.

Voss, K. J. & Zibordi, G. 1989 Radiometric and geometric calibration of a visible spectral electro-optic 'fish-eye' camera radiance distribution system. *J. Atmos. Oceanic Technol.* **6**, 652–662.

Walraven, R. L. 1981 Polarization imagery. *Opt. Engng* **20**, 14–18.

Wehner, R. 1976 Polarized-light navigation by insects. *Scient. Am.* **235**(1), 106–114.

Wehner, R. 1997 The ant's celestial compass system: spectral and polarization channels. In *Orientation and communication in arthropods* (ed. M. Lehrer), pp. 145–185. Basel: Birkhäuser.

Wolff, L. B. 1994 Polarization camera for computer vision with a beam splitter. *J. Opt. Soc. Am.* A **11**, 2935–2945.